JOURNAL OF GUIDANCE, CONTROL, AND DYNAMICS
Vol. 26, No. 3, May–June 2003

# Adaptive Neural Control of Deep-Space Formation Flying

Pini Gurfil*
*Princeton University, Princeton, New Jersey 08544*
Moshe Idan†
*Technion—Israel Institute of Technology, 32000 Haifa, Israel*
and
N. Jeremy Kasdin‡
*Princeton University, Princeton, New Jersey 08544*

**A novel nonlinear adaptive neural control methodology is presented for the challenging problem of deep-space spacecraft formation flying. When the framework of the circular restricted three-body problem with the sun and Earth as the primary gravitational bodies is utilized, a nonlinear model is developed that describes the relative formation dynamics. This model is not confined to the vicinity of the Lagrangian libration points but rather constitutes the most general nonlinear formulation. Then, a relative position controller is designed that consists of an approximate dynamic model inversion, linear compensation of the ideal feedback linearized model, and an adaptive neural-network-based element designed to compensate for the model inversion errors. The nominal dynamic inversion includes the gravitational forces, whereas the model inversion errors are assumed to stem from disturbances such as fourth-body gravitational effects and solar radiation pressure. The approach is illustrated by simulations, which confirm that the suggested methodology yields excellent tracking and disturbance rejection, thus, permitting submillimeter formation keeping precision.**

## Nomenclature

| | | |
|---|---|---|
| $\boldsymbol{d}$ | = | differential disturbance acceleration |
| $\boldsymbol{d}_M$ | = | moon's gravitational differential disturbance acceleration |
| $\boldsymbol{d}_{\mathrm{SP}}$ | = | solar radiation pressure differential disturbance acceleration |
| $\boldsymbol{e}$ | = | position tracking error |
| $K$ | = | optimal feedback gain matrix |
| $N_{\mathrm{inner}}$ | = | number of inner layer neurons |
| $Q_{\mathrm{lc}}$ | = | state weighting matrix for linear controller |
| $R_E$ | = | Earth radius |
| $R_{\mathrm{lc}}$ | = | pseudocontrol weighting matrix for linear controller |
| $\boldsymbol{r}$ | = | relative position |
| $\boldsymbol{r}_{\mathrm{tr}}$ | = | required relative position |
| $\boldsymbol{u}$ | = | differential control acceleration vector |
| $V$ | = | neural network input weighting matrix |
| $\boldsymbol{v}$ | = | relative velocity vector |
| $W$ | = | neural network output weighting matrix |
| $\boldsymbol{x}$ | = | relative state |
| $\beta$ | = | solar radiation pressure coefficient |
| $\boldsymbol{\Delta}$ | = | model inversion error |
| $\boldsymbol{\varepsilon}$ | = | state tracking error |
| $\zeta_{\mathrm{rm}}$ | = | damping coefficient of reference model |
| $\mu$ | = | normalized gravitational constant |
| $\mu_E$ | = | Earth gravitational constant |
| $\mu_S$ | = | sun gravitational constant |
| $\boldsymbol{\nu}$ | = | pseudocontrol vector |
| $\bar{\boldsymbol{\nu}}$ | = | neural network robustifying term |
| $\boldsymbol{\nu}_{\mathrm{lc}}$ | = | linear pseudocontrol signal |
| $\boldsymbol{\nu}_{\mathrm{ad}}$ | = | adaptive pseudocontrol signal |
| $\boldsymbol{\nu}_{\mathrm{tr}}$ | = | tracking pseudocontrol signal |
| $\sigma$ | = | sigmoid activation function |
| $\omega_{\mathrm{rm}}$ | = | natural frequency of reference model |

*Subscripts*

| | | |
|---|---|---|
| $l$ | = | leader spacecraft |
| $f$ | = | follower spacecraft |

## I. Introduction

SPACECRAFT formation flying (SFF) is an evolving technology for distributing the functionality of a single spacecraft between several closely flying satellites. This notion is expected to have the advantages of lower life-cycle cost, better performance, more adaptability to changing mission goals, and less susceptibility to the loss of individual satellites. Future applications of the SFF technology include high-resolution interferometry, stereographic imaging, synthetic apertures, and distinguishing spatial from temporal magnetospheric variations.

Formation flying missions can be categorized as Earth-centered and deep-space missions. The first category includes numerous missions such as TechSat21 (Ref. 1) and Earth Observing-1 (Ref. 2). The latter category includes long-baseline mid infrared interferometry missions such as the Terrestrial Planet Finder (TPF),[3] Starlight,[4] and Darwin[5]; x-ray interferometry missions such as the Micro-Arcsecond X-Ray Imaging Mission (MAXIM) Pathfinder[6]; and general relativity missions such as the Laser Interferometer Space Antenna (LISA).[7] In this work, deep-space formation flying is addressed.

The resolution and precision requirements associated with typical profiles of deep-space formation flying missions raise new challenges in trajectory design, control, instrumentation, and propulsion. The non-Keplerian trajectories of deep-space spacecraft necessitate a specialized treatment of the formation control, reorientation, and rotation. Often, trajectory analysis and design are carried out in the context of the circular restricted three-body problem (CR3BP) with the sun and the Earth as the primary gravitational bodies. This framework permits the derivation of mission-enabling trajectories such as halo orbits around the Lagrangian libration points,[3,8,9] out-of-ecliptic trajectories,[10] and distant retrograde orbits,[11] each

Received 28 January 2002; revision received 5 July 2002; accepted for publication 31 December 2002.

*Research Staff Member, Department of Mechanical and Aerospace Engineering; pgurfil@princeton.edu. Senior Member AIAA.
†Senior Lecturer, Faculty of Aerospace Engineering; moshe.idan@technion.ac.il. Associate Fellow AIAA.
‡Assistant Professor, Department of Mechanical and Aerospace Engineering; jkasdin@princeton.edu. Senior Member AIAA.

specifically suited to a different class of deep-space formation flying missions.

The aforementioned issues motivate the study of SFF control in arbitrary non-Keplerian orbits emerging from the CR3BP with the sun and Earth as the primaries. However, a complete analysis of SFF in arbitrary CR3BP trajectories must overcome several unique obstacles. Thus far, the vast majority of the studies dealing with formation flying adopted linear equations of motion found from local linearization about some reference trajectory. The resulting linear models are valid when dealing with both Earth-centered and libration point missions. In the former case, the well-known Clohessy–Wiltshire (CW) equations have been used (see Refs. 12–16). In the latter case, the equations of motion have been linearized about the $L_2$ libration point utilizing a CW-like reference frame and a periodic reference orbit.[9] However, future missions such as MAXIM Pathfinder, raise stringent submillimeter relative position control accuracy specifications that do not permit the utilization of linearization techniques.[17] Instead, the complete nonlinear models should be used, so that no approximation is involved in the design procedure.

Although most researchers have presented linearized SFF results, a few recently published works did consider nonlinear formation dynamics.[18–20] In Refs. 18 and 19, an Earth-centered SFF control design with a nonlinear gravitational field is presented. In Ref. 20, the Earth-centered case focusing on nonlinear $J_2$ perturbations is described again. However, all of these works neglected third-body effects. Others have provided means for analyzing configurations of spacecraft formations by neglecting the gravitational gradient and the solar radiation pressure.[21] These approaches constitute an unrealistic approximation when considering deep-space missions requiring highly precise position control.

In this paper, we address the complete nonlinear problem of deep-space formation flying and develop a control methodology that yields submillimeter formation keeping. Because of the formidable position control accuracy requirement, we do not linearize the problem, but rather model the complete highly nonlinear dynamics rendered by the CR3BP with the sun and the Earth as the primary gravitational bodies.

To prevent the microgravity deep-space environment from causing the spacecraft in the formation to drift apart, a novel closed-loop nonlinear position control law is developed that incorporates an adaptive disturbance rejection scheme for arbitrary reference trajectories. This approach is motivated by the recent advances in adaptive neural-network-(NN-) based control of nonlinear systems.[22–26] The methodology presented in this paper is an adaptation with appropriate extensions of those techniques for precise formation flying missions. In addition to controlling the formation on complex trajectories, this algorithm effectively compensates for deep-space disturbances such as solar radiation pressure (SRP) and fourth-body gravitation. These disturbances are incorporated into the analysis to illustrate the potency of the proposed control methodology to reject disturbances and cope with modeling errors.

The work presented herein focuses on the problem of developing a nonlinear control law for deep-space formation keeping assuming that the measurements required for its implementation are continuously available and ideal. This is the natural first step in developing a real-life control system. Once we quantify the extent to which the performance specifications using ideal measurements are achievable, future work will look into the effects of sensor errors and measurement rate on the overall formation keeping performance.

This paper starts by presenting the nonlinear equations of motion characterizing spacecraft dynamics in the CR3BP (Sec. II). We then develop an adaptive NN-based relative position controller that incorporates approximate dynamic model inversion and linear compensation of the ideal feedback linearized model (Sec. III). The nominal dynamic inversion includes the gravitational forces, whereas the model inversion errors are assumed to stem from disturbances such as fourth-body gravitational effects (for example, the moon) and SRP, or eccentricity effects of the Earth's orbit around the sun. The approach is illustrated by realistic nonlinear simulations, which confirm that the suggested methodology yields excellent tracking and disturbance rejection (Sec. IV). This paper further concludes that continuous-level plasma electric propulsion can be utilized to provide fine thrust for the microgravity environment of deep-space missions (Sec. V).

## II. Problem Formulation

There are two main approaches for the formulation of the spacecraft relative position control problem. The indirect approach is to station keep each spacecraft about some precalculated trajectory[9] that is chosen a priori to maintain some desired relative spacecraft position. The direct approach is to command the spacecraft to track a predefined relative reference trajectory, by selecting a (possibly virtual) leader spacecraft. This decentralized methodology is termed a formation keeping problem.[12–18] In this work, we adopt the direct approach, which has several considerable virtues. The most significant merit is that the leader does not have to station keep, which eliminates the need to equip it with a propulsion system. The leader spacecraft may, thus, be launched into an arbitrary, possibly Earth drift-away, trajectory.

For presentation simplicity, we consider a two-spacecraft formation, although the same formulation equally applies to formations of any size. To this end, let $\boldsymbol{r}_l$ and $\boldsymbol{r}_f \in \Re^3$ be the position vectors of the leader and follower spacecraft, respectively, relative to the Earth, $\boldsymbol{R} \in \Re^3$ that of the Earth relative to the sun, and $\boldsymbol{r} \in \Re^3$ the relative position vector between the leader and follower spacecraft, that is, $\boldsymbol{r}_f = \boldsymbol{r}_l + \boldsymbol{r}$ (Fig. 1). The inertial accelerations of the leader and follower spacecraft relative to Earth are given by[27]

$$\ddot{\boldsymbol{r}}_l = -\frac{\mu_E \boldsymbol{r}_l}{\|\boldsymbol{r}_l\|^3} - \left[\frac{\mu_S(\boldsymbol{R}+\boldsymbol{r}_l)}{\|\boldsymbol{R}+\boldsymbol{r}_l\|^3} - \frac{\mu_S \boldsymbol{R}}{\|\boldsymbol{R}\|^3}\right] + \boldsymbol{d}_l + \boldsymbol{u}_l \tag{1}$$

and

$$\ddot{\boldsymbol{r}}_l + \ddot{\boldsymbol{r}} = -\frac{\mu_E(\boldsymbol{r}_l+\boldsymbol{r})}{\|\boldsymbol{r}_l+\boldsymbol{r}\|^3} - \left[\frac{\mu_S(\boldsymbol{R}+\boldsymbol{r}_l+\boldsymbol{r})}{\|\boldsymbol{R}+\boldsymbol{r}_l+\boldsymbol{r}\|^3} - \frac{\mu_S \boldsymbol{R}}{\|\boldsymbol{R}\|^3}\right] + \boldsymbol{d}_f + \boldsymbol{u}_f \tag{2}$$

where $\mu_E$ and $\mu_S$ are the gravitational constants of the Earth and the sun, respectively, $\boldsymbol{d}_l$ and $\boldsymbol{d}_f \in \Re^3$ are disturbance acceleration vectors acting on the leader and follower, respectively, and $\boldsymbol{u}_l$ and $\boldsymbol{u}_f \in \Re^3$ are the control acceleration input vectors.

The equations of relative motion are obtained by subtracting Eq. (1) from Eq. (2), which yields

$$\ddot{\boldsymbol{r}} = \mu_E\left[\frac{\boldsymbol{r}_l}{\|\boldsymbol{r}_l\|^3} - \frac{\boldsymbol{r}_l+\boldsymbol{r}}{\|\boldsymbol{r}_l+\boldsymbol{r}\|^3}\right] + \mu_S\left[\frac{\boldsymbol{R}+\boldsymbol{r}_l}{\|\boldsymbol{R}+\boldsymbol{r}_l\|^3} - \frac{\boldsymbol{R}+\boldsymbol{r}_l+\boldsymbol{r}}{\|\boldsymbol{R}+\boldsymbol{r}_l+\boldsymbol{r}\|^3}\right] + \boldsymbol{d} + \boldsymbol{u} \tag{3}$$

where $\boldsymbol{u} = \boldsymbol{u}_f - \boldsymbol{u}_l$ and $\boldsymbol{d} = \boldsymbol{d}_f - \boldsymbol{d}_l$. The acceleration $\ddot{\boldsymbol{r}}$ is evaluated in a rotating Earth-fixed coordinate system $\hat{x}, \hat{y}, \hat{z}$, shown in Fig. 1. This coordinate system is different from the common reference frame[9] used to model the CR3BP. The basic notion is to choose

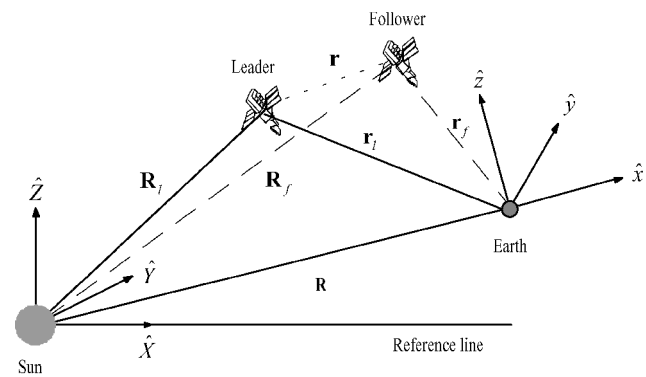


**Fig. 1 Coordinate systems: $\hat{x}, \hat{y}, \hat{z}$ define a rotating Earth-fixed coordinate system, and $\hat{X}, \hat{Y}, \hat{Z}$ is a heliocentric-ecliptic inertial frame.**

the origin of the coordinate system at the center of the small primary, Earth in our case, rather than the barycenter, and to normalize the masses by the mass of the large primary, the sun.[17,27] This coordinate system is useful from the engineering standpoint because the orbit determination process can be straightforwardly performed with the position and velocity vectors measured relative to Earth. Also, in a sense, this coordinate system is analogous to the CW reference frame in the two-body case, where the origin is set on the leader spacecraft.

Proceeding with the usual analysis but in this variant coordinate system, we shall use the following unit conventions. The position of the leader $\boldsymbol{r}_l = [x_l, y_l, z_l]^T$ and the relative position $\boldsymbol{r} = [x, y, z]^T$ are measured in astronomical units (AU), where the mean Earth–sun distance is $\|\boldsymbol{R}\| = 1$ AU $= 1.496 \times 10^8$ km. The time is normalized by the Earth mean heliocentric angular velocity, that is, $t = t^*/\sqrt{(\|\boldsymbol{R}\|^3/\mu_S)}$, where $t^*$ is the time measured in seconds. Accordingly, the velocity vector of the leader $\boldsymbol{v}_l = [\dot{x}_l, \dot{y}_l, \dot{z}_l]^T$ and the relative velocity $\boldsymbol{v} = [\dot{x}, \dot{y}, \dot{z}]^T$ are normalized by $\|\boldsymbol{R}\|/\sqrt{(\|\boldsymbol{R}\|^3/\mu_S)}$. The vectors $\boldsymbol{u} = [u_x, u_y, u_z]^T$ and $\boldsymbol{d} = [d_x, d_y, d_z]^T$ are normalized by $\mu_S/\|\boldsymbol{R}\|^2$. Also, let $\mu = \mu_E/(\mu_E + \mu_S) = 3.0034495182 \times 10^{-6}$.

The inertial reference frame used here is a heliocentric-ecliptic coordinate system, denoted by $\hat{X}, \hat{Y}, \hat{Z}$, as shown in Fig. 1. With utilization of the preceding unit convention, the transformation of some position vector $\boldsymbol{p}$ from the rotating frame to the inertial frame is given by

$$[\boldsymbol{p}]_{\hat{X},\hat{Y},\hat{Z}} = \begin{bmatrix} \cos t & -\sin t & 0 \\ \sin t & \cos t & 0 \\ 0 & 0 & 1 \end{bmatrix} \left\{ [\boldsymbol{p}]_{\hat{x},\hat{y},\hat{z}} + \begin{bmatrix} 1 \\ 0 \\ 0 \end{bmatrix} \right\} \tag{4}$$

Next, the acceleration of the leader from Eq. (1), $\ddot{\boldsymbol{r}}_l = [\ddot{x}_l, \ddot{y}_l, \ddot{z}_l]^T$, can be expressed in the rotating coordinate frame as

$$\ddot{x}_l = x_l + 2\dot{y}_l - \frac{\mu x_l}{\left(x_l^2 + y_l^2 + z_l^2\right)^{\frac{3}{2}}} - \frac{(1-\mu)(x_l+1)}{\left[(x_l+1)^2 + y_l^2 + z_l^2\right]^{\frac{3}{2}}} + 1 - \mu + d_{lx} + u_{lx} \tag{5}$$

$$\ddot{y}_l = y_l - 2\dot{x}_l - \frac{\mu y_l}{\left(x_l^2 + y_l^2 + z_l^2\right)^{\frac{3}{2}}} - \frac{(1-\mu) y_l}{\left[(x_l+1)^2 + y_l^2 + z_l^2\right]^{\frac{3}{2}}} + d_{ly} + u_{ly} \tag{6}$$

$$\ddot{z}_l = -\frac{\mu z_l}{\left(x_l^2 + y_l^2 + z_l^2\right)^{\frac{3}{2}}} - \frac{(1-\mu) z_l}{\left[(x_l+1)^2 + y_l^2 + z_l^2\right]^{\frac{3}{2}}} + d_{lz} + u_{lz} \tag{7}$$

where we substituted $\boldsymbol{d}_l = [d_{lx}, d_{ly}, d_{lz}]^T$ and $\boldsymbol{u}_l = [u_{lx}, u_{ly}, u_{lz}]^T$. Similarly, the relative acceleration $\ddot{\boldsymbol{r}} = [\ddot{x}, \ddot{y}, \ddot{z}]^T$ satisfies

$$\ddot{x} = x + 2\dot{y} + \mu \left[ \frac{x_l}{\left(x_l^2 + y_l^2 + z_l^2\right)^{\frac{3}{2}}} - \frac{x_l + x}{\left[(x_l+x)^2 + (y_l+y)^2 + (z_l+z)^2\right]^{\frac{3}{2}}} \right] + (1-\mu) \left[ \frac{1 + x_l}{\left[(x_l+1)^2 + y_l^2 + z_l^2\right]^{\frac{3}{2}}} - \frac{1 + x_l + x}{\left[(x_l+x+1)^2 + (y_l+y)^2 + (z_l+z)^2\right]^{\frac{3}{2}}} \right] + d_x + u_x \tag{8}$$

$$\ddot{y} = y - 2\dot{x} + \mu \left[ \frac{y_l}{\left(x_l^2 + y_l^2 + z_l^2\right)^{\frac{3}{2}}} - \frac{y_l + y}{\left[(x_l+x)^2 + (y_l+y)^2 + (z_l+z)^2\right]^{\frac{3}{2}}} \right] + (1-\mu) \left[ \frac{y_l}{\left[(x_l+1)^2 + y_l^2 + z_l^2\right]^{\frac{3}{2}}} - \frac{y_l + y}{\left[(x_l+x+1)^2 + (y_l+y)^2 + (z_l+z)^2\right]^{\frac{3}{2}}} \right] + d_y + u_y \tag{9}$$

$$\ddot{z} = \mu \left[ \frac{z_l}{\left(x_l^2 + y_l^2 + z_l^2\right)^{\frac{3}{2}}} - \frac{z_l + z}{\left[(x_l+x)^2 + (y_l+y)^2 + (z_l+z)^2\right]^{\frac{3}{2}}} \right] + (1-\mu) \left[ \frac{z_l}{\left[(x_l+1)^2 + y_l^2 + z_l^2\right]^{\frac{3}{2}}} - \frac{z_l + z}{\left[(x_l+x+1)^2 + (y_l+y)^2 + (z_l+z)^2\right]^{\frac{3}{2}}} \right] + d_z + u_z \tag{10}$$

To synthesize a relative position control law, it is convenient to utilize a state-space representation. To this end, we define the state vectors

$$\boldsymbol{x}_l \triangleq \left[\boldsymbol{r}_l^T, \boldsymbol{v}_l^T\right]^T = [x_l, y_l, z_l, \dot{x}_l, \dot{y}_l, \dot{z}_l]^T, \qquad \boldsymbol{x}_l \in \mathfrak{X}_l \subset \Re^6 \tag{11}$$

$$\boldsymbol{x} \triangleq \left[\boldsymbol{r}^T, \boldsymbol{v}^T\right]^T = [x, y, z, \dot{x}, \dot{y}, \dot{z}]^T, \qquad \boldsymbol{x}_l \in \mathfrak{X} \subset \Re^6 \tag{12}$$

where $\mathfrak{X}_l$ is a vector subspace of $\Re^6$ that satisfies the constraint $\|\boldsymbol{r}_l\| \geq R_E$, $\mathfrak{X}$ is a vector subspace of $\Re^6$ that satisfies $\|\boldsymbol{r}_l + \boldsymbol{r}\| \geq R_E$, and $R_E$ denotes Earth's radius.

When the definitions in Eqs. (11) and (12) are used Eqs. (5–10) are rewritten into state-space vector form:

$$\dot{\boldsymbol{x}}_l = A_{\text{lin}} \boldsymbol{x}_l + B \boldsymbol{g}_l(\boldsymbol{x}_l, \boldsymbol{u}_l, t) \tag{13}$$

$$\dot{\boldsymbol{x}} = A_{\text{lin}} \boldsymbol{x} + B \boldsymbol{g}(\boldsymbol{x}, \boldsymbol{x}_l, \boldsymbol{u}, t) \tag{14}$$

where

$$\boldsymbol{g}_l(\boldsymbol{x}_l, \boldsymbol{u}_l, t) = \boldsymbol{f}_l(\boldsymbol{x}_l) + \boldsymbol{d}_l(\boldsymbol{x}_l, t) + \boldsymbol{u}_l \tag{15}$$

$$\boldsymbol{g}(\boldsymbol{x}, \boldsymbol{x}_l, \boldsymbol{u}, t) = \boldsymbol{f}(\boldsymbol{x}, \boldsymbol{x}_l) + \boldsymbol{d}(\boldsymbol{x}, \boldsymbol{x}_l, t) + \boldsymbol{u} \tag{16}$$

and

$$A_{\text{lin}} = \begin{bmatrix} 0_{3\times3} & I_{3\times3} \\ A_{21} & A_{22} \end{bmatrix}, \qquad B = \begin{bmatrix} 0_{3\times3} \\ I_{3\times3} \end{bmatrix}$$

$$A_{21} = \begin{bmatrix} 1 & 0 & 0 \\ 0 & 1 & 0 \\ 0 & 0 & 0 \end{bmatrix}, \qquad A_{22} = \begin{bmatrix} 0 & 2 & 0 \\ -2 & 0 & 0 \\ 0 & 0 & 0 \end{bmatrix} \tag{17}$$

Here, $0_{3\times3}$ and $I_{3\times3}$ are the $3 \times 3$ zero and identity matrices, respectively. The nonlinear terms $\boldsymbol{f}_l(\boldsymbol{x}_l)$ and $\boldsymbol{f}(\boldsymbol{x}, \boldsymbol{x}_l)$ represent the gravitational acceleration of the leader and the differential gravitational acceleration, respectively, and are given by

$$\boldsymbol{f}_l(\boldsymbol{x}_l)=\begin{bmatrix} -\dfrac{\mu x_l}{\left(x_l^2+y_l^2+z_l^2\right)^{\frac{3}{2}}}-\dfrac{(1-\mu)(x_l+1)}{\left[(x_l+1)^2+y_l^2+z_l^2\right]^{\frac{3}{2}}}+1-\mu-\dfrac{\mu y_l}{\left(x_l^2+y_l^2+z_l^2\right)^{\frac{3}{2}}} \\ -\dfrac{(1-\mu)y_l}{\left[(x_l+1)^2+y_l^2+z_l^2\right]^{\frac{3}{2}}}-\dfrac{\mu z_l}{\left(x_l^2+y_l^2+z_l^2\right)^{\frac{3}{2}}}-\dfrac{(1-\mu)z_l}{\left[(x_l+1)^2+y_l^2+z_l^2\right]^{\frac{3}{2}}} \end{bmatrix} \tag{18}$$

$$\boldsymbol{f}(\boldsymbol{x},\boldsymbol{x}_l)=\begin{bmatrix} \mu\left[\dfrac{x_l}{\left(x_l^2+y_l^2+z_l^2\right)^{\frac{3}{2}}}-\dfrac{x_l+x}{\left[(x_l+x)^2+(y_l+y)^2+(z_l+z)^2\right]^{\frac{3}{2}}}\right] \\ +(1-\mu)\left[\dfrac{1+x_l}{\left[(x_l+1)^2+y_l^2+z_l^2\right]^{\frac{3}{2}}}-\dfrac{1+x_l+x}{\left[(x_l+x+1)^2+(y_l+y)^2+(z_l+z)^2\right]^{\frac{3}{2}}}\right] \\ \mu\left[\dfrac{y_l}{\left(x_l^2+y_l^2+z_l^2\right)^{\frac{3}{2}}}-\dfrac{y_l+y}{\left[(x_l+x)^2+(y_l+y)^2+(z_l+z)^2\right]^{\frac{3}{2}}}\right] \\ +(1-\mu)\left[\dfrac{y_l}{\left[(x_l+1)^2+y_l^2+z_l^2\right]^{\frac{3}{2}}}-\dfrac{y_l+y}{\left[(x_l+x+1)^2+(y_l+y)^2+(z_l+z)^2\right]^{\frac{3}{2}}}\right] \\ \mu\left[\dfrac{z_l}{\left(x_l^2+y_l^2+z_l^2\right)^{\frac{3}{2}}}-\dfrac{z_l+z}{\left[(x_l+x)^2+(y_l+y)^2+(z_l+z)^2\right]^{\frac{3}{2}}}\right] \\ +(1-\mu)\left[\dfrac{z_l}{\left[(x_l+1)^2+y_l^2+z_l^2\right]^{\frac{3}{2}}}-\dfrac{z_l+z}{\left[(x_l+x+1)^2+(y_l+y)^2+(z_l+z)^2\right]^{\frac{3}{2}}}\right] \end{bmatrix} \tag{19}$$

where $\boldsymbol{f}_l\colon \mathfrak{X}\to\Re^3$ and $\boldsymbol{f}\colon \Re^3\to\Re^3$.

To complete the modeling of the system dynamics, a description of possible disturbances is required. However, the disturbance model is used for simulation purposes only because of the inherent uncertainties in the disturbance model and because the control law cannot precisely predict them. Thus, the actual controller design scheme assumes no knowledge of the disturbance model. Its effect on the formation keeping dynamics is compensated adaptively in real-time operation. Consequently, we postpone the presentation of the disturbance model to Sec. IV. The only assumption made regarding the disturbance vector, denoted by $\boldsymbol{d}(\boldsymbol{x},\boldsymbol{x}_l,t)$, is that it is norm bounded, that is,

$$\|\boldsymbol{d}(\boldsymbol{x},\boldsymbol{x}_l,t)\|\le D \tag{20}$$

Note that Eq. (20) does not restrict the generality of the treatment because, physically speaking, deep-space disturbances (namely, fourth-body gravity effects and solar radiation pressure) are always bounded.

## III. Relative Position Control

Assume that we wish to steer the follower spacecraft to track some reference trajectory relative to the leader spacecraft. This trajectory may represent some optimal relative maneuver, a predefined time-varying relative trajectory or simply a constant offset. In general, the controlled variables of the relative state are the position components, that is,

$$\boldsymbol{r}=H\boldsymbol{x}=[I_{3\times 3}\quad 0_{3\times 3}]\boldsymbol{x} \tag{21}$$

and the required relative trajectory is given by $\boldsymbol{r}_{\mathrm{tr}}(t)=[x_{\mathrm{tr}}(t),\ y_{\mathrm{tr}}(t),\ z_{\mathrm{tr}}(t)]^T$.

Note that the position of the leader, $\boldsymbol{r}_l$, constitutes an exogenous signal to the equations of the relative dynamics [Eqs. (14)]. Because the controlled dynamics are those of the relative motion, the particular nature of the leader trajectory is of no importance for the treatment to follow, as long as it is known and bounded.

To develop a robust control of the relative position between spacecraft in the presence of unknown disturbances, we have utilized a nonlinear control methodology, which will be detailed. The relative position control loop developed hereafter is described schematically in Fig. 2. It consists of an approximate dynamic model inversion, linear compensation of the ideal feedback linearized model, and an adaptive NN-based element designed to compensate for the model inversion errors. In the current work, a full state controller is designed, with the assumption of the availability of the measurement of both the relative position and velocity vectors and the position and velocity of the leader relative to the Earth. This implies that the relevant information is shared between the leader and follower spacecraft.

Note that the particular control design approach presented in this section has been adopted because of its modular structure, ease of design and implementation, and excellent performance. Furthermore, it has been shown to work where the linearized formation flying methodology failed to yield the required formation keeping precision; see Ref. 17 for details. Although no claim is being made regarding the optimality of the approach, simulations will show that the derived controller performs well in terms of fuel expenditure.

### A. Approximate Feedback Linearization via Dynamic Inversion

The dynamic model inversion is performed on the nonlinear elements of Eq. (14). We define a pseudocontrol signal as

$$\boldsymbol{\nu}=\hat{\boldsymbol{g}}(\boldsymbol{x},\boldsymbol{x}_l,\boldsymbol{u})=\hat{\boldsymbol{f}}(\boldsymbol{x},\boldsymbol{x}_l)+\boldsymbol{u} \tag{22}$$

where $\hat{\boldsymbol{f}}(\boldsymbol{x},\boldsymbol{x}_l)$ is an estimate of $\boldsymbol{f}(\boldsymbol{x},\boldsymbol{x}_l)$.

Substituting Eq. (22) into Eq. (14) leads to

$$\dot{\boldsymbol{x}}=A_{\mathrm{lin}}\boldsymbol{x}+B[\boldsymbol{\nu}+\boldsymbol{\Delta}(\boldsymbol{x},\boldsymbol{x}_l,t)] \tag{23}$$

where $\boldsymbol{\Delta}(\boldsymbol{x},\boldsymbol{x}_l,t)$ is the model inversion error, given by

$$\boldsymbol{\Delta}(\boldsymbol{x},\boldsymbol{x}_l,t)=\boldsymbol{f}(\boldsymbol{x},\boldsymbol{x}_l)-\hat{\boldsymbol{f}}(\boldsymbol{x},\boldsymbol{x}_l)+\boldsymbol{d}(\boldsymbol{x},\boldsymbol{x}_l,t) \tag{24}$$

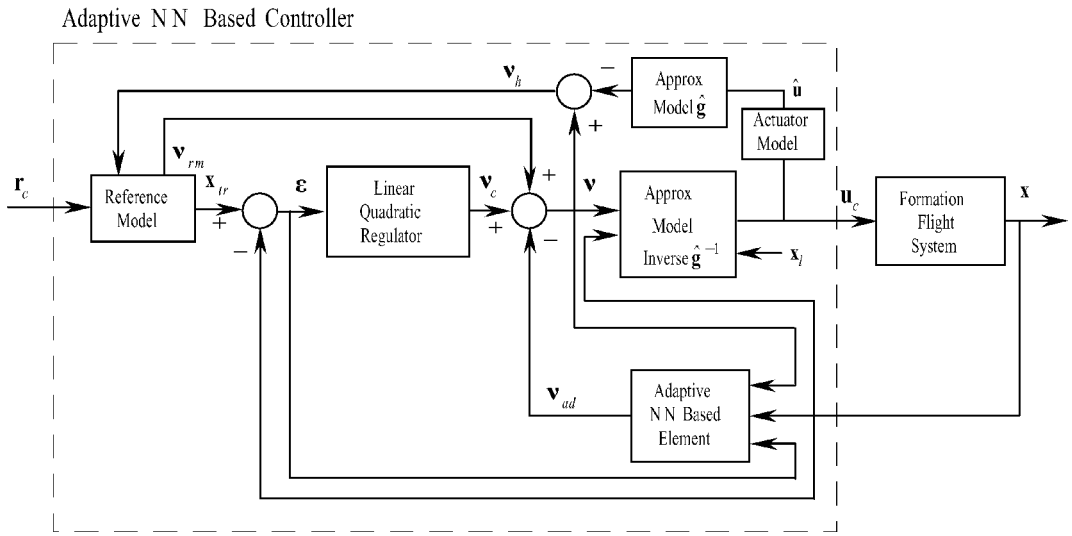


**Fig. 2 Block diagram of the relative position control loop.**

Thus, the model inversion error stems from two sources: modeling/measurement inaccuracies, $\boldsymbol{f}(\boldsymbol{x}, \boldsymbol{x}_l) - \hat{\boldsymbol{f}}(\boldsymbol{x}, \boldsymbol{x}_l)$, and exogenous disturbances, $\boldsymbol{d}(\boldsymbol{x}, \boldsymbol{x}_l, t)$. Modeling/measurement inaccuracies may stem from several factors. The most obvious error source is due to inaccuracies in the state measurement required to obtain $\hat{\boldsymbol{f}}(\boldsymbol{x}, \boldsymbol{x}_l)$. However, as already mentioned, we shall assume here ideal and continuous measurements. Nevertheless, modeling errors may still occur. For example, if $\boldsymbol{f}(\boldsymbol{x}, \boldsymbol{x}_l)$ includes only gravitational terms, as the case discussed here, modeling inaccuracies will result from neglecting the eccentricity of Earth's orbit. Moreover, if $\boldsymbol{f}(\boldsymbol{x}, \boldsymbol{x}_l)$ is augmented to include a nominal SRP term, inaccuracies will result from the uncertainty in the SRP coefficient. If it is assumed that there are no modeling inaccuracies, Eq. (24) reduces to $\boldsymbol{\Delta}(\boldsymbol{x}, \boldsymbol{x}_l, t) = \boldsymbol{d}(\boldsymbol{x}, \boldsymbol{x}_l, t)$, that is, the model inversion error includes the disturbance terms only, some of which may be unknown and/or unmodeled.

The pseudocontrol $\boldsymbol{\nu}$ of Eq. (22) is designed such that satisfactory dynamic characteristics and tracking performance are achieved despite the modeling errors and disturbances, or, equivalently, despite the model inversion error $\boldsymbol{\Delta}(\boldsymbol{x}, \boldsymbol{x}_l, t)$. Once $\boldsymbol{\nu}$ is computed, the actual control signal is obtained by inverting Eq. (22), that is,

$$\boldsymbol{u} = \boldsymbol{\nu} - \hat{\boldsymbol{f}}(\boldsymbol{x}, \boldsymbol{x}_l) \tag{25}$$

which clearly depends on the measurements of $\boldsymbol{x}$ and $\boldsymbol{x}_l$. According to the preceding requirements, $\boldsymbol{\nu}$ is comprised of three major elements: 1) $\boldsymbol{\nu}_{\text{lc}}$, a linear compensation term designed to achieve the desired dynamic characteristics of the ideal linear model, while neglecting the gravity and disturbance accelerations; 2) $\boldsymbol{\nu}_{\text{tr}}$, used to achieve tracking of the relative reference trajectory or regulation to a constant set point and a function of $\boldsymbol{r}_{\text{tr}}$ and its derivatives; and 3) $\boldsymbol{\nu}_{\text{ad}}$, an adaptive signal designed to compensate for the effect of the model inversion error $\boldsymbol{\Delta}(\boldsymbol{x}, \boldsymbol{x}_l, t)$.

Thus, $\boldsymbol{\nu}$ is chosen as

$$\boldsymbol{\nu} = \boldsymbol{\nu}_{\text{lc}} + \boldsymbol{\nu}_{\text{tr}} - \boldsymbol{\nu}_{\text{ad}} \tag{26}$$

Substituting Eq. (26) into Eq. (23) leads to

$$\dot{\boldsymbol{x}} = A_{\text{lin}}\boldsymbol{x} + B\{\boldsymbol{\nu}_{\text{lc}} + \boldsymbol{\nu}_{\text{tr}} + [\boldsymbol{\Delta}(\boldsymbol{x}, \boldsymbol{x}_l, t) - \boldsymbol{\nu}_{\text{ad}}]\} \tag{27}$$

### B. Linear Controller Design

A linear full state feedback controller is designed to provide the desired dynamic characteristics of the ideal gravity and disturbance-free linear model, obtained by neglecting the model inversion error and the other components of the pseudocontrol signal $\boldsymbol{\nu}$ in Eq. (27). Any linear control design technique can be used for the controller design problem associated with this linear model. In the current study, we adopted the optimal linear quadratic regulation (LQR) approach that provides a straightforward formulation of the tradeoff between control effort and response time. Thus, $\boldsymbol{\nu}_{\text{lc}}$ is chosen to minimize the infinite-horizon cost functional

$$\boldsymbol{J} = \int_{t_0}^{\infty} \left(\boldsymbol{x}^T Q_{\text{lc}}\boldsymbol{x} + \boldsymbol{\nu}_{\text{lc}}^T R_{\text{lc}}\boldsymbol{\nu}_{\text{lc}}\right) \mathrm{d}t \tag{28}$$

The optimization results in the standard linear control solution given by

$$\boldsymbol{\nu}_{\text{lc}} = -K\boldsymbol{x} = -K_1\boldsymbol{r} - K_2\boldsymbol{v} \tag{29}$$

Substituting Eq. (29) into Eq. (27) leads to

$$\dot{\boldsymbol{x}} = A_{\text{cl}}\boldsymbol{x} + B\{\boldsymbol{\nu}_{\text{tr}} + [\boldsymbol{\Delta}(\boldsymbol{x}, \boldsymbol{x}_l, t) - \boldsymbol{\nu}_{\text{ad}}]\} \tag{30}$$

where the closed-loop dynamics matrix $A_{\text{cl}}$ is given by

$$A_{\text{cl}} = A_{\text{lin}} - BK = \begin{bmatrix} 0_{3\times 3} & I_{3\times 3} \\ A_{21}^{\text{cl}} & A_{22}^{\text{cl}} \end{bmatrix} \tag{31}$$

with

$$A_{21}^{\text{cl}} = A_{21} - K_1, \qquad A_{22}^{\text{cl}} = A_{22} - K_2 \tag{32}$$

The LQR technique guarantees stability of the closed-loop system, ensuring that $A_{\text{cl}}$ is Hurwitz.

Next, the reference trajectory related signal $\boldsymbol{\nu}_{\text{tr}}$ is chosen so that the linear formulation of the closed-loop tracking error dynamics does not involve specifically $\boldsymbol{r}_{\text{tr}}$ and its derivative. To that end, $\boldsymbol{\nu}_{\text{tr}}$ is set as

$$\boldsymbol{\nu}_{\text{tr}} = \ddot{\boldsymbol{r}}_{\text{tr}} - A_{21}^{\text{cl}}\boldsymbol{r}_{\text{tr}} - A_{22}^{\text{cl}}\dot{\boldsymbol{r}}_{\text{tr}} \tag{33}$$

The position tracking error and the combined position and velocity tracking errors are defined as

$$\boldsymbol{e} \triangleq \boldsymbol{r}_{\text{tr}} - \boldsymbol{r} \tag{34}$$

$$\boldsymbol{\varepsilon} \triangleq [\boldsymbol{e}^T \quad \dot{\boldsymbol{e}}^T]^T \tag{35}$$

A routine manipulation of Eqs. (31–36) leads to the tracking error dynamics equation

$$\dot{\boldsymbol{\varepsilon}} = A_{\text{cl}}\boldsymbol{\varepsilon} + B[\boldsymbol{\nu}_{\text{ad}} - \boldsymbol{\Delta}(\boldsymbol{x}, \boldsymbol{x}_l, t)] \tag{36}$$

which in fact is not forced by $\boldsymbol{r}_{\text{tr}}$ and its derivatives.

From Eq. (33) it is evident that the first and second time derivative of the reference trajectory are needed to generate $\boldsymbol{\nu}_{\text{tr}}$. To that end, we

introduce a second-order reference model for generating the relative reference trajectory $\boldsymbol{r}_{\text{tr}}$ and its time derivatives. The reference model, driven by an external command signal $\boldsymbol{r}_c$, can be expressed as

$$\ddot{\boldsymbol{r}}_{\text{tr}} = \omega_{\text{rm}}^2 \boldsymbol{r}_c - \omega_{\text{rm}}^2 \boldsymbol{r}_{\text{tr}} - 2\zeta_{\text{rm}}\omega_{\text{rm}}\dot{\boldsymbol{r}}_{\text{tr}} \tag{37}$$

where $\omega_{\text{rm}}$ and $\zeta_{\text{rm}}$ are the natural frequency and the damping coefficient of the model, specifying its dynamic characteristics.

It is convenient to combine and regroup the expressions for $\boldsymbol{\nu}_{\text{lc}}$ and $\boldsymbol{\nu}_{\text{tr}}$ of Eqs. (29) and (33), respectively, as follows

$$\boldsymbol{\nu}_{\text{lc}} + \boldsymbol{\nu}_{\text{tr}} = \underbrace{K_1\boldsymbol{e} + K_2\dot{\boldsymbol{e}}}_{\nu_c} + \underbrace{\ddot{\boldsymbol{r}}_{\text{tr}} - A_{21}\boldsymbol{r}_{\text{tr}} - A_{22}\dot{\boldsymbol{r}}_{\text{tr}}}_{\nu_{\text{rm}}} \tag{38}$$

where $\boldsymbol{\nu}_c$ is the redefined output of the linear controller operating on the tracking error only and $\boldsymbol{\nu}_c$ depends only on the outputs of the reference model. The last two terms are used in the actual controller implementation, in which the pseudocontrol $\boldsymbol{\nu}$ is redefined as

$$\boldsymbol{\nu} = \boldsymbol{\nu}_c + \boldsymbol{\nu}_{\text{rm}} - \boldsymbol{\nu}_{\text{ad}} \tag{39}$$

### C. NN for Inversion Error Compensation

The next step is synthesizing $\boldsymbol{\nu}_{\text{ad}}$, the adaptive signal designed to compensate for the effect of the model inversion error $\boldsymbol{\Delta}(\boldsymbol{x}, \boldsymbol{x}_l, t)$. To this end, a nonlinear single hidden layer (SHL) NN is used. The SHL NN was chosen due to its universal approximation property.[28,29]

For an input vector $\bar{\boldsymbol{x}}$, which is constructed of the measured states, the reference model outputs and the pseudocontrol signal, the output of the SHL NN is given by

$$\boldsymbol{\nu}_{\text{ad}} = W^T\boldsymbol{\sigma}(\boldsymbol{z}) + \bar{\boldsymbol{\nu}} \tag{40}$$

where $\boldsymbol{z} = V^T\bar{\boldsymbol{x}}$, $V$ is the input weighting matrix, $W$ is the output weighting matrix, and $\bar{\boldsymbol{\nu}}$ is a so-called robustifying term. For $N_{\text{inner}}$ inner layer neurons, $\boldsymbol{\sigma} = [\sigma_1, \sigma_2, \ldots, \sigma_{N_{\text{inner}}}]^T$ is a vector of sigmoid activation functions, whose elements are given by

$$\sigma_i = 1/(1 + e^{-a_i z_i}), \qquad i = 1, 2, \ldots, N_{\text{inner}} \tag{41}$$

where $a_i$, $i = 1, 2, \ldots, N_{\text{inner}}$, are arbitrarily chosen activation potentials.

Although ideal weighting matrices are unknown and usually cannot be computed, they can be estimated (or "learned") in real time using the following NN weights training rules[22,26]:

$$\dot{W} = -\left[(\boldsymbol{\sigma}(\boldsymbol{z}) - J(\boldsymbol{z})V^T\bar{\boldsymbol{x}})\boldsymbol{\eta} + \kappa\|\boldsymbol{\eta}\|W\right]\boldsymbol{\Gamma}_W \tag{42}$$

$$\dot{V} = -\Gamma_V[\bar{\boldsymbol{x}}\boldsymbol{\eta}W^T J(\boldsymbol{z}) + \kappa\|\boldsymbol{\eta}\|V] \tag{43}$$

where $\Gamma_W$ and $\Gamma_V$ are positive definite learning rate matrices, $J(\boldsymbol{z})$ is the diagonal Jacobian matrix $J(\boldsymbol{z}) = \partial\boldsymbol{\sigma}(\boldsymbol{z})/\partial\boldsymbol{z}$ evaluated at the current value of $\boldsymbol{z}$, and $\kappa$ is the $e$-modification parameter. Here, $\boldsymbol{\eta}$ is defined by

$$\boldsymbol{\eta} = \boldsymbol{\varepsilon}^T PB \tag{44}$$

where $P \succ 0$ is a positive definite solution of the Lyapunov equation

$$A_{\text{cl}}^T P + PA_{\text{cl}} + Q = 0 \tag{45}$$

for any positive definite $Q \succ 0$.

The robustifying term $\bar{\boldsymbol{\nu}}$ is given by

$$\bar{\boldsymbol{\nu}} = -K_Z\left(\|Z\|_F + Z_M^*\right)\boldsymbol{\eta}^T \tag{46}$$

where

$$Z = \begin{bmatrix} W & 0 \\ 0 & V \end{bmatrix} \tag{47}$$

and $\|\cdot\|_F$ is a Frobenius norm of a matrix and $Z_M^*$ is a bound on the ideal (unknown) NN weights $Z^*$, that is, $\|Z^*\|_F \le Z_M^*$.

### D. Control Constraints and Pseudocontrol Hedging

The thrust required for formation flying in deep-space missions is usually characterized by a vast dynamic range.[17] A milli-Newton thrust is required for rapid repositioning, whereas micro-Newton thrust is required for steady-state formation keeping. The only systems currently envisioned that can be used to provide the required thrust are electric or plasma electric propulsion devices, such as Hall thrusters, field emission electric propulsion or pulsed plasma thrusters.[30] These devices are characterized by maximum and minimum thrust levels. Thus, the control vector is constrained by the inequalities

$$u_{\min,i} \le u_i \le u_{\max,i}, \qquad i = 1, \ldots, n_u \tag{48}$$

where $n_u$ is the number of activated thrusters.

NN training difficulties may occur when actuator saturation is encountered, possibly leading to NN wind-up. This is attributed to that actuator saturation, which changes the dynamic input–output characteristics of the system, may be interpreted by the NN as a change in the system dynamics and, thus, a change in the model inversion error $\boldsymbol{\Delta}$. The pseudocontrol hedging (PCH) methodology is introduced to address these adaptation difficulties within a model reference adaptive control (MRAC) architecture.[31] The main notion of PCH is to limit or hedge the reference model of MRAC architecture to prevent the NN from adapting to saturations when those are encountered. PCH does not affect the NN adaptation to other sources of inversion error for which compensation is possible.

Conceptually, PCH moves the reference model backward by an estimated deficit in the performed vs commended pseudocontrol action caused by actuator saturation. In effect, the reference model, which produces the commanded pseudocontrol, is limited or hedged according to the difference between the commanded and actually achieved pseudocontrol. Consequently, with PCH, the NN is trained correctly using only achievable pseudocontrol signals.

The actuator command is determined by Eq. (25), while neglecting the actuator saturation. This is stated as

$$\boldsymbol{u}_{\text{cmd}} = \boldsymbol{\nu} - \hat{\boldsymbol{f}}(\boldsymbol{x}, \boldsymbol{x}_l) \tag{49}$$

Because of saturation, the actual actuator action $\boldsymbol{u}$ will not equal to its commanded value $\boldsymbol{u}_{\text{cmd}}$. Consequently, a pseudocontrol hedge signal $\boldsymbol{\nu}_h$ is defined as the difference between the commanded pseudocontrol input and the actually achieved pseudocontrol, which may be nonzero when an actuator is saturated. To compute this difference, a measurement or an estimate of the actuator position $\hat{\boldsymbol{u}}$ is required. This estimate, chosen simply as the saturated command, is then used to compute the pseudocontrol hedge as

$$\boldsymbol{\nu}_h = \hat{\boldsymbol{g}}(\boldsymbol{x}, \boldsymbol{x}_l, \boldsymbol{u}_{\text{cmd}}) - \hat{\boldsymbol{g}}(\boldsymbol{x}, \boldsymbol{x}_l, \hat{\boldsymbol{u}}) = \boldsymbol{u}_{\text{cmd}} - \hat{\boldsymbol{u}} \tag{50}$$

where $\hat{\boldsymbol{g}}$ is an estimate of $\boldsymbol{g}$ and the last equality in Eq. (50) results from the definition of $\hat{g}$ given in Eq. (22). The PCH signal is next introduced as an additional input into the reference model, forcing it to move back. If the reference model update without PCH is given by Eq. (37), then the reference model update with PCH is redefined as

$$\ddot{\boldsymbol{r}}_{\text{tr}} = \omega_{\text{rm}}^2 \boldsymbol{r}_c - \omega_{\text{rm}}^2 \boldsymbol{r}_{\text{tr}} - 2\zeta_{\text{rm}}\omega_{\text{rm}}\dot{\boldsymbol{r}}_{\text{tr}} - \boldsymbol{\nu}_h \tag{51}$$

The instantaneous pseudocontrol signal $\boldsymbol{\nu}_{\text{rm}}$, defined in Eq. (38), is not changed by PCH, that is, it is computed using $\ddot{\boldsymbol{r}}_{\text{tr}}$ of Eq. (37), leading to

$$\boldsymbol{\nu}_{\text{rm}} = \left(\omega_{\text{rm}}^2 \boldsymbol{r}_c - \omega_{\text{rm}}^2 \boldsymbol{r}_{\text{tr}} - 2\zeta_{\text{rm}}\omega_{\text{rm}}\dot{\boldsymbol{r}}_{\text{tr}}\right) - A_{21}\boldsymbol{r}_{\text{tr}} - A_{22}\dot{\boldsymbol{r}}_{\text{tr}} \tag{52}$$

where the terms in the parentheses constitute the unhedged $\ddot{\boldsymbol{r}}_{\text{tr}}$. This formulation of $\boldsymbol{\nu}_{\text{rm}}$ is required for successful stability analysis of NN-based adaptive control with PCH, detailed in Ref. 31. Hence, the effect of the PCH signal on the pseudocontrol is introduced only through the reference model dynamics.

## IV. Simulation

In this section the mentioned ideas are illustrated by simulation. The simulation is based on the equations of motion presented in Sec. II, the control methodology developed in Sec. III, and a disturbance model, to be presented shortly. The disturbance model represents perturbing forces typical to the deep-space environment. One must consider gravitational forces from other celestial bodies. For the type of trajectories considered here, the moon constitutes the main gravitational perturbation. SRP is another disturbance to account for. Other disturbances, such as Earth's magnetic field, its oblateness, and the atmospheric drag are not pertinent to the deep-space environment and are, thus, neglected.

It is important to understand the role of disturbances in the forthcoming analysis. Theoretically, every disturbance that can be modeled may be inverted using a feedback linearization methodology as was implemented on the Earth and the sun gravitational forces. The role of the disturbances in our case, however, is to illustrate the capability of the controller to reject unknown or uncertain disturbances, or, in the more general sense, to perform robustly under the presence of model inversion errors. To this end, the moon and the SRP disturbances are used as model inversion error "generators." The nominal model of the moon's disturbance and the SRP are known. However, there is always a degree of uncertainty either in the moon's phase relative to Earth or the SRP constant. Thus, instead of inverting the nominal part of these disturbances and employing the NN element to reject only the uncertain portion, we have trained the NN to reject the overall disturbance signals. This was done to illustrate the capability of the algorithm to deal with large model inversion errors that, in the real case, may stem from, for example, the measurement process (sensor noise, bias, sampling rate) or actuator imperfections (thrust noise, misalignments, nonlinearities).

Thus, the control law is aimed at guaranteeing robust precision formation flight while rejecting the disturbances not accounted for in the inverting controller, by using the adaptive NN element. Note that the NN is trained online only and has no direct information regarding the nature of the disturbances except that they are bounded [Eq. (20)].

### A. Disturbance Model

Let us first consider the gravitational disturbance of the moon. The acceleration of the leader and the follower due to the moon are given by

$$\boldsymbol{d}_{Ml} = -\frac{\mu_M(\boldsymbol{R}_M + \boldsymbol{r}_l)}{\|\boldsymbol{R}_M + \boldsymbol{r}_l\|^3} + \frac{\mu_M \boldsymbol{R}_M}{\|\boldsymbol{R}_M\|^3} \tag{53}$$

$$\boldsymbol{d}_{Mf} = -\frac{\mu_M(\boldsymbol{R}_M + \boldsymbol{r}_l + \boldsymbol{r})}{\|\boldsymbol{R}_M + \boldsymbol{r}_l + \boldsymbol{r}\|^3} + \frac{\mu_M \boldsymbol{R}_M}{\|\boldsymbol{R}_M\|^3} \tag{54}$$

respectively, where $\boldsymbol{R}_M$ is the position vector of the moon relative to Earth and $\mu_M$ is the gravitational constant of the moon. We idealize the moon's orbit as a circle of radius $\|\boldsymbol{R}_M\| = 0.002569\,\text{AU} = 384{,}320$ km in the ecliptic plane. (Actually, the Moon's orbit is inclined $5^\circ 09'$ to the ecliptic. For the treatment to follow, this inclination can be safely neglected.) The phase of the moon in this orbit is $\theta$. Under these conditions, the normalized disturbance exerted by the moon on the leader spacecraft is expressed in a vector form as

$$\boldsymbol{d}_{Ml}(\boldsymbol{x}_l, t) = \begin{bmatrix} \dfrac{-\mu_1[x_l + \|\boldsymbol{R}_M\|\cos(\omega_M t + \theta)]}{\left[(x_l + \|\boldsymbol{R}_M\|\cos(\omega_M t + \theta))^2 + (y_l + \|\boldsymbol{R}_M\|\sin(\omega_M t + \theta))^2 + z_l^2\right]^{\frac{3}{2}}} + \dfrac{\mu_1 \cos(\omega_M t + \theta)}{\|\boldsymbol{R}_M\|^2} \\ \dfrac{-\mu_1[y_l + \|\boldsymbol{R}_M\|\sin(\omega_M t + \theta)]}{\left[(x_l + \|\boldsymbol{R}_M\|\cos(\omega_M t + \theta))^2 + (y_l + \|\boldsymbol{R}_M\|\sin(\omega_M t + \theta))^2 + z_l^2\right]^{\frac{3}{2}}} + \dfrac{\mu_1 \sin(\omega_M t + \theta)}{\|\boldsymbol{R}_M\|^2} \\ \dfrac{-\mu_1 z_l}{\left[(x_l + \|\boldsymbol{R}_M\|\cos(\omega_M t + \theta))^2 + (y_l + \|\boldsymbol{R}_M\|\sin(\omega_M t + \theta))^2 + z_l^2\right]^{\frac{3}{2}}} \end{bmatrix} \tag{55}$$

where $\omega_M = \sqrt{(\mu_M/\mu_S \cdot \|\boldsymbol{R}\|^3/\|\boldsymbol{R}_M\|^3)}$ and $\mu_1 = \mu_M/\mu_S$.

Therefore, the differential disturbance vector is

$$\boldsymbol{d}_M(\boldsymbol{x}, \boldsymbol{x}_l, t) = \begin{bmatrix} \dfrac{\mu_1[x_l + \|\boldsymbol{R}_M\|\cos(\omega_M t + \theta)]}{\left[(x_l + \|\boldsymbol{R}_M\|\cos(\omega_M t + \theta))^2 + (y_l + \|\boldsymbol{R}_M\|\sin(\omega_M t + \theta))^2 + z_l^2\right]^{\frac{3}{2}}} \\ \quad - \dfrac{\mu_1[x + x_l + \|\boldsymbol{R}_M\|\cos(\omega_M t + \theta)]}{\left[(x + x_l + \|\boldsymbol{R}_M\|\cos(\omega_M t + \theta))^2 + (y + y_l + \|\boldsymbol{R}_M\|\sin(\omega_M t + \theta))^2 + (z + z_l)^2\right]^{\frac{3}{2}}} \\ \dfrac{\mu_1[y_l + \|\boldsymbol{R}_M\|\sin(\omega_M t + \theta)]}{\left[(x_l + \|\boldsymbol{R}_M\|\cos(\omega_M t + \theta))^2 + (y_l + \|\boldsymbol{R}_M\|\sin(\omega_M t + \theta))^2 + z_l^2\right]^{\frac{3}{2}}} \\ \quad - \dfrac{\mu_1[y + y_l + \|\boldsymbol{R}_M\|\sin(\omega_M t + \theta)]}{\left[(x + x_l + \|\boldsymbol{R}_M\|\cos(\omega_M t + \theta))^2 + (y + y_l + \|\boldsymbol{R}_M\|\sin(\omega_M t + \theta))^2 + (z + z_l)^2\right]^{\frac{3}{2}}} \\ \dfrac{\mu_1 z_l}{\left[(x_l + \|\boldsymbol{R}_M\|\cos(\omega_M t + \theta))^2 + (y_l + \|\boldsymbol{R}_M\|\sin(\omega_M t + \theta))^2 + z_l^2\right]^{\frac{3}{2}}} \\ \quad - \dfrac{\mu_1(z + z_l)}{\left[(x + x_l + \|\boldsymbol{R}_M\|\cos(\omega_M t + \theta))^2 + (y + y_l + \|\boldsymbol{R}_M\|\sin(\omega_M t + \theta))^2 + (z + z_l)^2\right]^{\frac{3}{2}}} \end{bmatrix} \tag{56}$$

Next, we consider the SRP disturbance. To this end, we adopt a widely used model.[32] According to this model, the leader acceleration due to SRP is

$$\boldsymbol{d}_{\mathrm{SP}l} = -\left(\beta_l \big/ \|\boldsymbol{R}_l\|^2\right)(\hat{\boldsymbol{R}}_l \cdot \boldsymbol{n})^2 \boldsymbol{n} \tag{57}$$

where $\beta_l$ is a parameter that depends on the coefficient of reflectivity, the area and mass of the spacecraft, the solar flux, and the speed of light. $\boldsymbol{R}_l = \boldsymbol{R} + \boldsymbol{r}_l$ (Fig. 1) is the position vector of the leader relative to the sun, $\hat{\boldsymbol{R}}_l \triangleq \boldsymbol{R}_l / \|\boldsymbol{R}_l\|$, and $\boldsymbol{n}$ is the attitude vector of the spacecraft in the rotating frame.

To simplify Eq. (57), we assume that $\boldsymbol{n} = \hat{\boldsymbol{R}}_l$, which yields

$$\boldsymbol{d}_{\mathrm{SP}l} = -\left(\beta_l \boldsymbol{R}_l \big/ \|\boldsymbol{R}_l\|^3\right) \tag{58}$$

Componentwise, Eq. (58) may be rewritten as

$$\boldsymbol{d}_{\mathrm{SP}l}(\boldsymbol{x}_l) = -\beta_l \begin{bmatrix} \dfrac{1 + x_l}{\left[(1 + x_l)^2 + y_l^2 + z_l^2\right]^{\frac{3}{2}}} \\ \dfrac{y_l}{\left[(1 + x_l)^2 + y_l^2 + z_l^2\right]^{\frac{3}{2}}} \\ \dfrac{z_l}{\left[(1 + x_l)^2 + y_l^2 + z_l^2\right]^{\frac{3}{2}}} \end{bmatrix} \tag{59}$$

The same procedure can be repeated for the follower spacecraft yielding

$$\boldsymbol{d}_{\mathrm{SP}f} = -\left(\beta_f \boldsymbol{R}_f \big/ \|\boldsymbol{R}_f\|^3\right) \tag{60}$$

where $\beta_f$ is the SRP of the follower and $\boldsymbol{R}_f = \boldsymbol{R} + \boldsymbol{r}_f = \boldsymbol{R} + \boldsymbol{r}_l + \boldsymbol{r}$ (Fig. 1). The SRP disturbance vector exerted on the follower, thus, may be written as

$$\boldsymbol{d}_{\mathrm{SP}f}(\boldsymbol{x}_l, \boldsymbol{x}) = -\beta_f \begin{bmatrix} \dfrac{1 + x_l + x}{\left[(1 + x_l + x)^2 + (y_l + y)^2 + (z_l + z)^2\right]^{\frac{3}{2}}} \\ \dfrac{y_l + y}{\left[(1 + x_l + x)^2 + (y_l + y)^2 + (z_l + z)^2\right]^{\frac{3}{2}}} \\ \dfrac{z_l + z}{\left[(1 + x_l + x)^2 + (y_l + y)^2 + (z_l + z)^2\right]^{\frac{3}{2}}} \end{bmatrix} \tag{61}$$

Thus, the differential SRP disturbance is given by

$$\begin{aligned} \boldsymbol{d}_{\mathrm{SP}}(x, x_l) &= \boldsymbol{d}_{\mathrm{SP}f}(x, x_l) - \boldsymbol{d}_{\mathrm{SP}l}(x, x_l) \\ &= \beta_l \begin{bmatrix} \dfrac{1 + x_l}{(1 + x_l)^{\frac{3}{2}}} \\ \dfrac{y_l}{y_l^{\frac{3}{2}}} \\ \dfrac{z_l}{z_l^{\frac{3}{2}}} \end{bmatrix} - \beta_f \begin{bmatrix} \dfrac{1 + x_l + x}{(1 + x_l)^{\frac{3}{2}}} \\ \dfrac{y_l + y}{(y_l + y)^{\frac{3}{2}}} \\ \dfrac{z_l + z}{(z_l + z)^{\frac{3}{2}}} \end{bmatrix} \end{aligned} \tag{62}$$

Finally, the total differential disturbance acceleration is given by

$$\boldsymbol{d}(\boldsymbol{x}, \boldsymbol{x}_l) = \boldsymbol{d}_M(\boldsymbol{x}, \boldsymbol{x}_l) + \boldsymbol{d}_{\mathrm{SP}}(\boldsymbol{x}, \boldsymbol{x}_l) \tag{63}$$

### B. Simulation Scenario and Numerical Values

We start by presenting the leader's trajectory, shown in Fig. 3. We assume that the constellation is initially parked at a 200-km low Earth orbit. Then, an impulsive velocity change of $\Delta v = 4.9$ km/s is used to inject the spacecraft into an out-of-ecliptic Earth drift-away

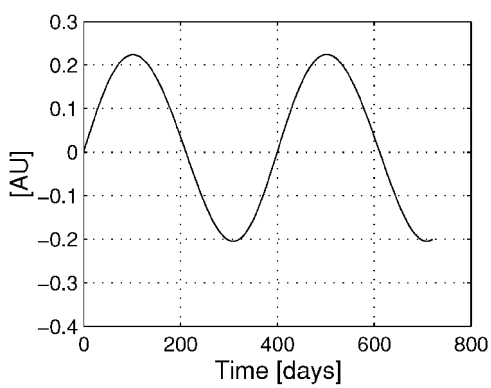


a) Leader normal displacement $z_l$

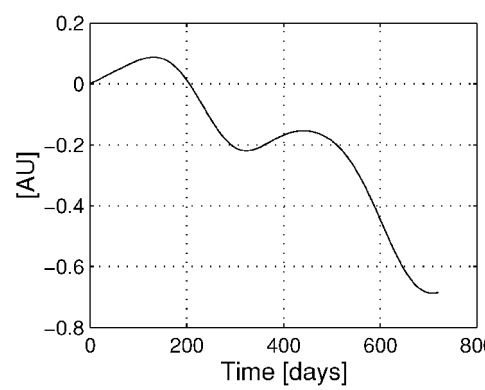


c) Leader radial displacement $x_l$

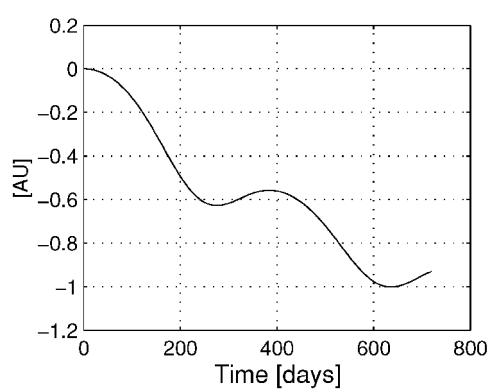


b) Leader transverse displacement $y_l$

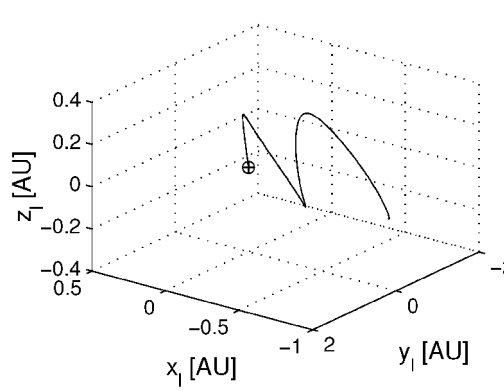


d) Three-dimensional leader trajectory

**Fig. 3 Leader trajectory in the Earth-fixed rotating frame.**

trajectory.[10] During a two-year mission lifetime (selected merely as a benchmark), the maximum normal deflection of the trajectory above the ecliptic is 0.223 AU, and the maximum distance from Earth is 1.2 AU. The resulting leader trajectory in the inertial frame is a non-Keplerian orbit with the leader's distance from the sun satisfying $0.986\ \text{AU} \leq \|\boldsymbol{R}_l\| \leq 1.138\text{AU}$.

The formation is initialized arbitrarily at $[x(0), y(0), z(0), \dot{x}(0), \dot{y}(0), \dot{z}(0)]^T = [5, 5, 5, 0, 0, 0]^T$ m. The reference trajectory is aimed at separating the spacecraft to a constant distance of $\|\boldsymbol{r}(t_f)\| = 450$ km, a very long baseline taken from NASA's MAXIM Pathfinder mission.[6] In spite of the large baseline, MAXIM Pathfinder requires submillimeter formation keeping. These numbers were chosen here to illustrate the ability of the proposed controller to provide precision formation keeping even under such stringent requirements. The final position components were thus, selected as $x(t_f) = y(t_f) = z(t_f) = 450/\sqrt{3}$ km.

The next step was performing feedback linearization and closing an LQR control loop on the feedback-linearized system as described in Sec. III. We have selected the values $Q_{\text{lc}} = 2 \cdot 10^5 \times I_{6\times 6}$ and $R_{\text{lc}} = 30 \cdot I_{3\times 3}$. (Note that the diagonal terms of these matrices are dimensionless, due to the use of normalized variables.) The SRP parameters were calculated assuming that the solar flux is $F_S = 1358$ W/m$^2$, the speed of light is $c = 3 \times 10^8$ m/s, the mass of each spacecraft is $m = 500$ kg, the cross-sectional area is

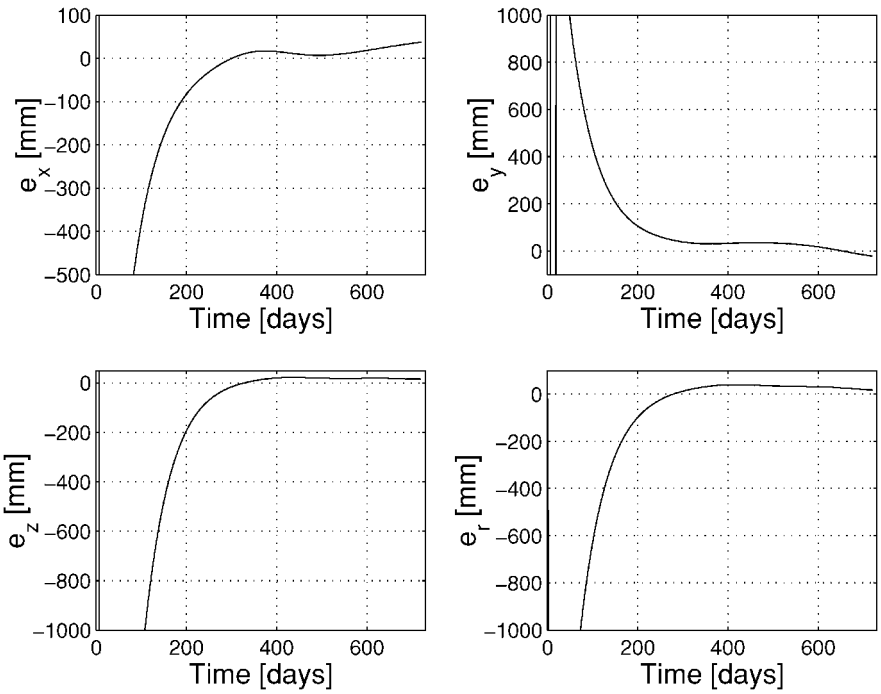


**Fig. 4 Tracking error components and relative range tracking error without NN compensation assume values between 100 mm and about 1 m due to the moon's gravitational disturbance and the differential SRP.**

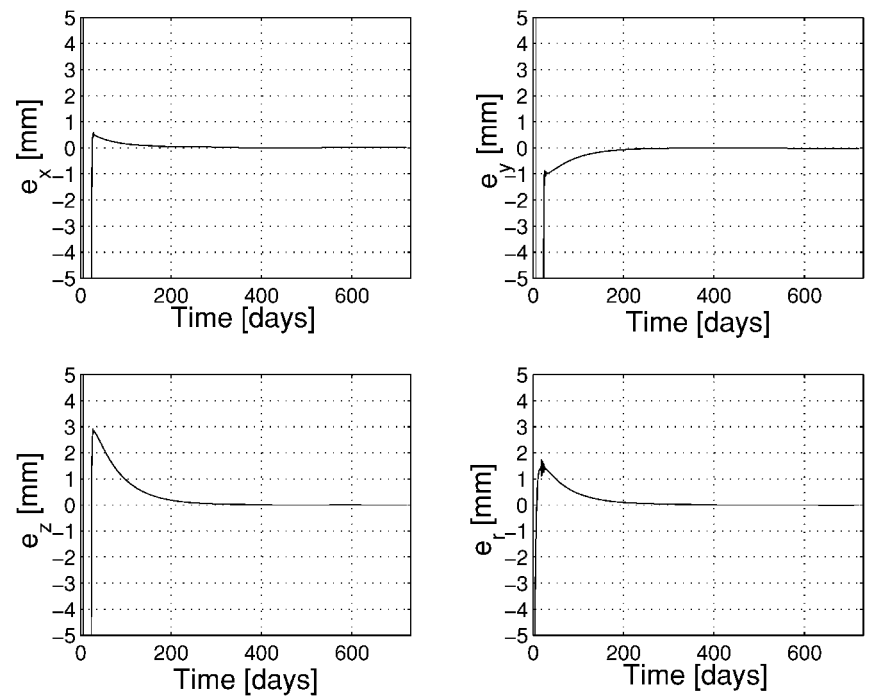


**Fig. 5 Tracking error components and relative range tracking error with adaptive NN compensation are dramatically reduced to below 5 mm after 4 days and to a submillimeter level after 50 days.**

$S = 3.5$ m$^2$, and the coefficient of reflectivity is $q = 0.6$, which results in $\beta_l = SF_S(1+q)/(mc) = \beta_f = 5 \times 10^{-8}$ m/s$^2$. The PCH algorithm was implemented assuming that each thruster is capable of providing a maximum of 1 mN of thrust, so that the total thrust is limited to 1.732 mN. The lower thrust limit was assumed to be 0.

### C. Results

The first simulation run of the closed-loop position control system was performed without the adaptive NN disturbance rejection element, $\nu_{\text{ad}} \equiv 0$, using the approximate model inversion and LQ components of the controller. The tracking components, $e_x$, $e_y$, and $e_z$, as well as the relative distance tracking error $e_r \triangleq \|\boldsymbol{r}_{\text{tr}}\| - \|\boldsymbol{r}\|$ are shown in Fig. 4. Note that these variables are given in units of millimeters. Noticeably, the tracking errors range between 100 mm and 1 m, due to the moon and SRP disturbances. After 200 days, the relative distance tracking error is about $-100$ mm. At the end of mission lifetime, this tracking error is about 18 mm. This performance was achieved with a proper tuning of $Q_{\text{lc}}$ and $R_{\text{lc}}$, but due to the control

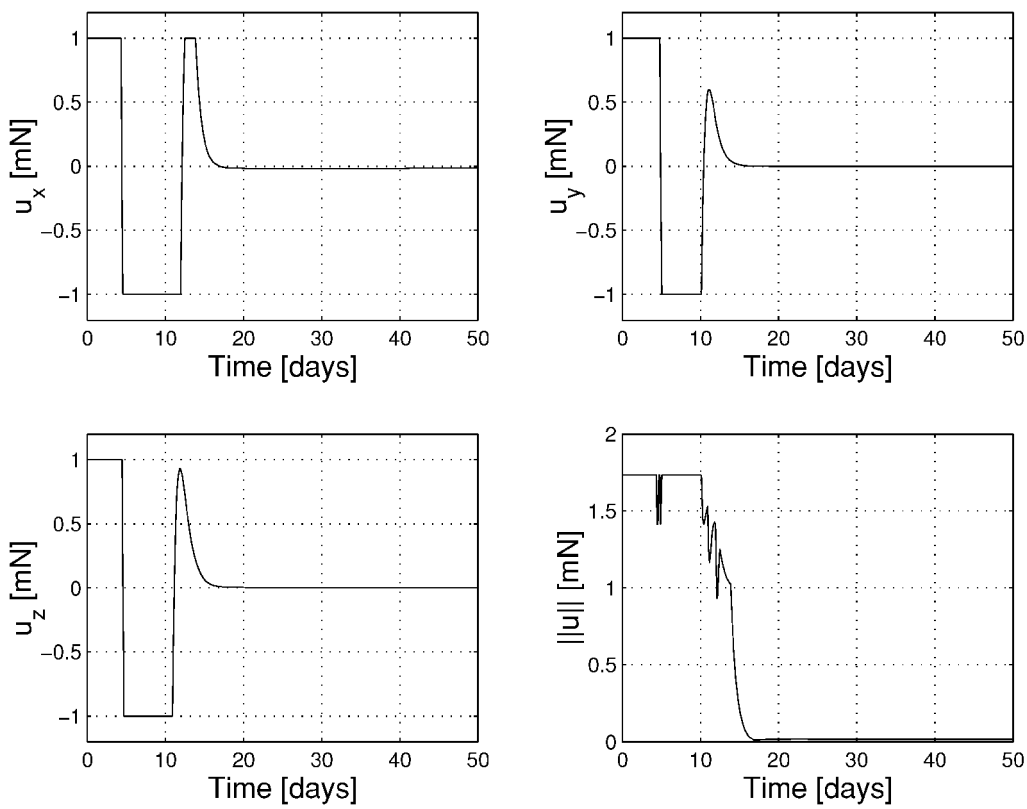


**Fig. 6 Thrust components and total thrust during the first 50 days of the mission; maximum total thrust during the transient phase limited to 1.732 mN; required thrust for formation keeping drops to the micro-Newton level after about 20 days.**

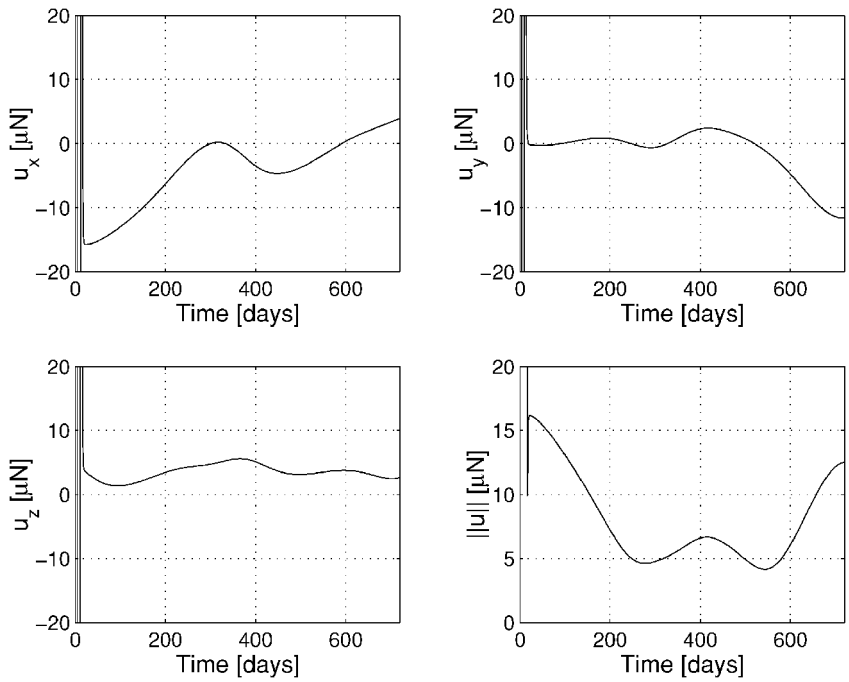


**Fig. 7 Thrust components and total thrust for the entire mission; required thrust for formation keeping ranges from 5 to 15 $\mu$N.**

saturation, this accuracy falls quite short of achieving submillimeter formation keeping and is by no means feasible for the specific mission considered here. However, the picture dramatically changes when the NN element is employed. Coupled with the feedback linearized LQR controlled closed-loop system, excellent formation keeping is obtained. Figure 5 presents the tracking error components in the latter case. The tracking errors drop by approximately three orders of magnitude, thus, enabling submillimeter precision. The relative distance tracking error crosses a 5-mm threshold after about 4 days, and achieves a submillimeter level after approximately 50 days.

We conclude this section by examining the thrust required for formation keeping. The thrust components, $u_x$, $u_y$, and $u_z$, as well as the total thrust $\|\boldsymbol{u}\|$ are shown in Figs. 6 and 7. Figure 6 shows the thrust components and the total thrust during the first 50 days of the mission. The maximum total thrust during the transient phase is limited to 1.732 mN. The required thrust for formation keeping drops to the micro-Newton level after about 20 days. Figure 7 shows the micro-Newton thrusting phase of the mission, which requires between 5 and 15 $\mu$N of thrust. These numbers yield a total $\Delta V$ of about 5 m/s for the entire mission lifetime. This minuscule $\Delta V$ value indicates that the proposed controller, although not designed as a fuel-optimal controller, renders a very small control effort.

## V. Conclusions

This paper presented a novel nonlinear adaptive deep-space formation flying control methodology. We used the general framework of the restricted three-body problem to formulate nonlinear relative dynamics.

Based on the realistic simulations described, we may draw a few important conclusions. First, solar radiation pressure and the moon's gravitational perturbations considerably influence the relative trajectory of the spacecraft and, thus, should not be overlooked when high-precision missions are concerned. The controller developed here, however, has been extremely successful in rejecting these exogenous disturbances. This implies that an onboard implementation of the algorithm, assuming availability of accurate measurements, may provide submillimeter formation flying performance despite modeling errors, an important result for future deep-space missions.

Second, the overall control effort required was very small, which implies that a modest amount of propellant may be carried. It is concluded that the proposed control architecture is fuel feasible, although it was not derived based on fuel optimization.

Third, in accordance with previous works, a large dynamic range is needed from the actuators: A milli-Newton thrust is required for rapid repositioning, whereas micro-Newton thrust is required for steady-state formation keeping. The required thrust may be generated by a combination of several plasma/electric propulsion systems, such as Hall thrusters, field emission electric propulsion or pulsed plasma thrusters.

Preliminary simulations show that the formation keeping control system is robust to sensor noise. However, further study is required to complete the development for the case of nonideal measurements.

## Acknowledgment

The contributions of the first and third authors were supported by the NASA Goddard Space Flight Center under Grant NAG-10933.

## References

[1]Das, A., and Cobb, R., "TechSat 21-Space Missions Using Collaborating Constellations of Satellites," *Proceedings of the 12th AIAA/USU Annual Conference on Small Satellites*, AIAA, Reston, VA, 1998.

[2]Folta, D., and Quinn, D., "Enhanced Formation Flying for the Earth Observing-1 (EO-1) New Millennium Mission," *Proceeding of the Flight Mechanics Symposium*, NASA Goddard Space Flight Center, Greenbelt, MD, 1997, pp. 405, 406.

[3]*Terrestrial Planet Finder*, NASA/Jet Propulsion Lab. Publ. 99-3, California Inst. of Technology, Pasadena, CA, May 1999.

[4]NASA Origins, URL: http://origins.jpl.nasa.gov [cited 1 Dec. 2001].

[5]Darwin, URL: http://ast.star.rl.ac.uk/darwin [cited 1 Dec. 2001].

[6]MAXIM Pathfinder, URL: http://maxim.gsfc.nasa.gov/docs/pathfinder/pathfinder.html [cited 1 Dec. 2001].

[7]LISA, URL: http://lisa.jpl.nasa.gov [cited 1 Dec. 2001].

[8]Howell, K. C., Barden, B. T., and Lo., M. W., "Application of Dynamical Systems Theory to Trajectory Design for a Libration Point Mission," *Journal of the Astronautical Sciences*, Vol. 45, No. 2, 1997, pp. 161–178.

[9]Folta, D., and Carpenter, J. R., "Formation Flying with Decentralized Control in Libration Point Orbits," *Proceedings of International Symposium on Space Dynamics*, CNES, Paris, France, 2000, pp. 217–227.

[10]Gurfil, P., and Kasdin, N. J., "Optimal Out-of-the-Ecliptic Trajectories for Space-Borne Observatories," *Proceedings of the 11th AAS/AIAA Space Flight Mechanics Meeting*, AIAA, Reston, VA, 2001, pp. 833–865.

[11]Ocampo, C. A., and Rosborough, G. W., "Transfer Trajectories for Distant Retrograde Orbiters of the Earth," American Astronautical Society, Paper AAS 93-180, 1993.

[12]Yeh, H. H., Nelson, E., and Sparks, A., "Nonlinear Tracking Control for Satellite Formations," *Journal of Guidance, Control, and Dynamics*, Vol. 25, No. 2, 2002, pp. 376–386.

[13]Kapila, V., Sparks, A. G., and Buffington, J. M., "Spacecraft Formation Flying: Dynamics and Control," *Journal of Guidance, Control, and Dynamics*, Vol. 23, No. 3, 2000, pp. 561–564.

[14]Ulybyshev, Y., "Long-Term Formation Keeping of Satellite Constellation Using Linear-Quadratic Controller," *Journal of Guidance, Control, and Dynamics*, Vol. 21, No. 1, 1998, pp. 109–115.

[15]Vassar, R. H., and Sherwood, R. B., "Formationkeeping for a Pair of Satellites in a Circular Orbit," *Journal of Guidance, Control, and Dynamics*, Vol. 8, No. 2, 1985, pp. 235–242.

[16]Inalhan, G., Tillerson, M., and How, J. P., "Relative Dynamics and Control of Spacecraft Formations in Eccentric Orbits," *Journal of Guidance, Control, and Dynamics*, Vol. 25, No. 1, 2002, pp. 48–60.

[17]Gurfil, P., and Kasdin, N. J., "Dynamics and Control of Spacecraft Formation Flying in Three-Body Trajectories," *Proceedings of the 2001 AIAA Guidance, Navigation and Control Conference*, AIAA, Reston, VA, 2001.

[18]de Querioz, M. S., Kapila, V., and Yan, Q., "Adaptive Nonlinear Control of Multiple Spacecraft Formation Flying," *Journal of Guidance, Control, and Dynamics*, Vol. 23, No. 3, 2000, pp. 385–390.

[19]Irvin, D. J., and Jacques, D. R., "Linear vs. Nonlinear Control Techniques for the Reconfiguration of Satellite Formations," *Proceedings of the 2001 AIAA Guidance, Navigation and Control Conference*, AIAA, Reston, VA, 2001.

[20]Alfriend, K. T., and Schaub, H., "Dynamics and Control of Spacecraft Formations: Challenges and Some Solutions," *Journal of the Astronautical Science*, Vol. 48, No. 2, 2000, pp. 249–267.

[21]Wang, P. K. C., and Hadaegh, F. Y., "Minimum-Fuel Formation Reconfiguration of Multiple Free-Flying Spacecraft," *Journal of the Astronautical Science*, Vol. 47, No. 1, 1999, pp. 77–102.

[22]Lewis, F. L., Yesildirek, A., and Liu, K., "Multilayer Neural-Net Robot Controller with Guaranteed Tracking Performance," *IEEE Transactions on Neural Networks*, Vol. 7, No. 2, 1996, pp. 388–399.

[23]Kim, B. S., and Calise, A. J., "Nonlinear Flight Control Using Neural Networks," *Journal of Guidance, Control, and Dynamics*, Vol. 20, No. 1, 1997, pp. 26–33.

[24]Kim, Y., and Lewis, F., *High-Level Feedback Control with Neural Networks*, World Scientific, River Edge, NJ, 1998.

[25]Lewis, F., "Nonlinear Network Structures for Feedback Control," *Asian Journal of Control*, Vol. 1, No. 4, 1999, pp. 205–228.

[26]Rysdyk, R., and Calise, A. J., "Nonlinear Adaptive Flight Control Using Neural Networks," *IEEE Controls Systems Magazine*, Vol. 18, No. 6, 1998, pp. 812–818.

[27]Breakwell, J. V., "Trajectories Launched Normal to the Ecliptic," *Proceedings of the 14th International Astronautical Congress*, CNES, Toulouse, France, 1963, pp. 128–141.

[28]Funahashi, K., "On the Approximate Realization of Continuous Mappings by Neural Networks," *Neural Networks*, Vol. 2, No. 3, 1989, pp. 183–192.

[29]Hornik, K., Stinchcombe, M., and White, H., "Multilayer Feedforward Networks Are Universal Approximators," *Neural Networks*, Vol. 2, No. 4, 1989, pp. 359–366.

[30]Polzin, K. A., Choueiri, E. Y., Gurfil, P., and Kasdin, N. J., "Comparative Study of Plasma Propulsion Requirements for TPF Architectures: Free-Flying, Monolithic and Tethered," *Proceedings of the 37th AIAA/ASME/SAE/ASEE Joint Propulsion Conference*, AIAA, Reston, VA, 2001.

[31]Johnson, E., "Limited Authority Adaptive Flight Control," Ph.D. Dissertation, Dept. of Aerospace Engineering, Georgia Inst. of Technology, Atlanta, GA, 2000.

[32]McInnes, C. R., Simmons, J. F., and MacDonald, E. W., "Solar Sail Parking in Restricted Three-Body Systems," *Journal of Guidance, Control, and Dynamics*, Vol. 17, No. 2, 1994, pp. 399–406.